Stanford Exploration Project, Report 94, November 11, 1997, pages 1–326

Seismic anisotropy in Trinidad: Processing and interpretation

Tariq Alkhalifah[1] *and Dave Rampton*[2]

keywords: *anisotropy, processing, interpretation*

ABSTRACT

The lithology of offshore Trinidad is formed of alternating sequences of sand and shale dominated layers. Average (effective) anisotropy is much lower in Trinidad compared to the prevoiusly studied area of offshore Angola due to the large amount of sand in the subsurface. Nevertheless, accounting for anisotropy in seismic processing results in improved imaging of structural and stratigraphic features. The imaging improvement is shown for two different lines from that region. Inversion for an interval value of the anisotropy parameter (η), suggests that low values are correlated with sands (or any other isotropic material), while high interval η values are correlated with shales. Correlation between separate independent measurements for η across common midpoints (CMPs) enhances the credibility of such estimates as a representation of real geologic parameters. Finally, the η curve agrees well with gamma-ray well-log measurements used as a shale estimate. This result confirms the hypothesis that anisotropy is due to shales in the subsurface, and the inversion for interval η can subsequently be used to predict lithology.

INTRODUCTION

The presence of anisotropy in the subsurface is now widely recognized, and the importance of handling it in the processing stage for improved imaging is gaining momentum. However, the feasibility of using inverted anisotropic parameters to understand the underlying lithology is yet to be evaluated. This paper tackles this important issue; specifically we will attempt to use inverted anisotropic parameters estimated using surface seismic data to discriminate between sands and shales.

Alkhalifah and Tsvankin (1995) demonstrated that, for transversely isotropic (TI)

[1]**email**:tariq@sep.stanford.edu

[2]Amoco Trinidad Oil Company, 501 WestLake Park Boulevard, Houston, TX 77079-2696, **email**:dcrampton@amoco.com

media with vertical symmetry axis (VTI media), just *two* parameters are sufficient for performing all time-related processing such as NMO correction (including non-hyperbolic moveout correction, if necessary), DMO correction, and prestack and poststack time migration. Taking V_h to be the P-wave velocity in the horizontal direction, one of these two parameters, η, is given by

$$\eta \equiv 0.5 \left(\frac{V_h^2}{V_{\rm nmo}^2(0)} - 1 \right) = \frac{\epsilon - \delta}{1 + 2\delta}\,, \tag{1}$$

and the other, the short-spread normal moveout (NMO) velocity for a horizontal reflector, is given by

$$V_{\rm nmo}(0) = V_{P0}\sqrt{1 + 2\delta}\,, \tag{2}$$

where V_{P0} is the P-wave vertical velocity, and ϵ and δ are Thomsen's (1986) dimensionless anisotropy parameters.

These two parameters can also be characterized directly in terms of the conventional elastic coefficients c_{ij} as follows

$$\eta = \frac{c_{11}(c_{33} - c_{44})}{2c_{13}(c_{13} + 2c_{44}) + 2c_{33}c_{44}} - \frac{1}{2},$$

and

$$V_{\rm nmo}(0) = \sqrt{\frac{c_{13}(c_{13} + 2c_{44}) + c_{33}c_{44}}{(c_{33} - c_{44})}}.$$

The fact that we cannot uniquely determine the elastic coefficients from η and $V_{\rm nmo}(0)$ does not matter, because time-related processing depends on just $V_{\rm nmo}(0)$ and η.

Alkhalifah and Tsvankin (1995) further show that these two parameters, η and $V_{\rm nmo}(0)$, can be obtained solely from surface seismic P-wave data, using estimates of stacking velocity for reflections from interfaces having two distinct dips. The inversion technique discussed by Alkhalifah and Tsvankin, however, is designed for a homogeneous medium above the reflector, while realistic subsurface models are, at a minimum, vertically inhomogeneous. Later, Alkhalifah (1997a) modified their inversion to handle vertically inhomogeneous media. Here, η, whose departure from zero indicates anisotropy, is the key parameter that we will use for the lithology discrimination.

Using data from offshore Africa, Alkhalifah (1997a) showed that anisotropic processing yields improved images over that obtained from isotropic processing. Reflections from dipping faults that were attenuated in the isotropically-processed data appeared in the anisotropic one. Reflections from horizontal events also benefitted from the non-hyperbolic correction imbedded in the anisotropic processing.

Here, we show that the importance of anisotropy processing is not confined to data from offshore Africa. Imnage of data from offshore Trinidad can also be improved with processing that takes the anisotropy of the subsurface into account. Unlike the shale-dominated subsurface in offshore Angola, the subsurface in Trinidad is made up of alternating sequences of sand and shale. However, significant improvement in imaging using anisotropic processing is demonstrated in Trinidad. In addition, the inversion of the anisotropic data makes it possible to evaluate the feasibility of distinguishing between shale-dominated layers and sand-dominated layers, due to the physical property that shales have inherent anisotropy while sands do not.

TRINIDAD DATA

Offshore Trinidad sediment are the result of clastics sediments from the Orinoco River in Venezuela. The high rate of sediment influx results in thick clastic sequences with a mixture of sands and shales. Because of the large amount of sand, the influence of anisotropy in the region is less evident than in data from the western African region (Alkhalifah, 1997a). Nevertheless, taking anisotropy into account yields better images, as well as better understanding of the subsurface lithology.

The first line of seismic data shown in this paper was acquired as a 2-D line in 1984 in the regional dip direction (confirmed from 3-D data). The line is approximately 30 km long with a source-to-receiver spacing ratio of 2. As a result, the maximum fold in the data is 60 and the maximum offset acquired, 3200 m, is lower than what is typically acquired nowadays. Such offsets are, nevertheless, sufficient for applying the dip-moveout inversion of Alkhalifah (1997a) since this method does not require long offsets. However, the non-hyperbolic inversion of Alkhalifah (1997b) is not appropriate for this data since this inversion relies on the availability of large offsets. The peak frequency in the data is around 30 Hz.

The second line of data from the Trinidad region is newer data (acquired in 1989), with offsets that extend to 6 km. This 2-D line was also acquired in the regional subsurface dip direction. The source-to-receiver spacing ratio here is 3, and the maximum fold in the data is 90. Due to the large offsets acquired, the more flexible non-hyperbolic inversion is used on this data. The peak frequency for this data is closer to 40 Hz.

ANISOTROPY PROCESSING

Two assumptions are made here: first, rays traveling through the subsurface are confined to the vertical plane that contains the sources and receivers (a 2-D assumption). Second, no lateral velocity variation exists in the region of the analysis (a time-processing assumption). However, some treatment to lateral inhomogeneity is applied in the NMO correction stage. Violating the first assumption will degrade the anisotropic processing result and generally reduce the degree of anisotropy measured. Therefore, measurements from out-of-plane reflections will not be mistaken for anisotropy (Lynn et. al., 1991). If anything, measurements from out-of-plane reflections will lower the value of η due to the lower NMO velocities associated with out-of-plane reflections. Violating the second assumption will result in errors similar to those encountered using isotropic time processing in areas of lateral inhomogeneity. These errors are dependent on the degree of lateral inhomogeneity, and as is likely here, such errors are expected to be small.

The first line

Figure 1 shows a zero-offset section from offshore Trinidad that contains reflections from a large number of dipping faults. Amoco Trinidad Exploration provided the seismic data and the stacking velocities. The section was processed using a conventional 2-D isotropic processing sequence that included a conventional NMO (using the stacking velocities that Amoco provided), followed by a log-stretch (Notfors and Godfrey, 1987) version of Hale's (1984) DMO. Anisotropy is expected to vary with depth due to the alternating sand-dominated and shale-dominated layers. Shales are believed to be the main source of anisotropy in sedimentary basins (Banik, 1984).

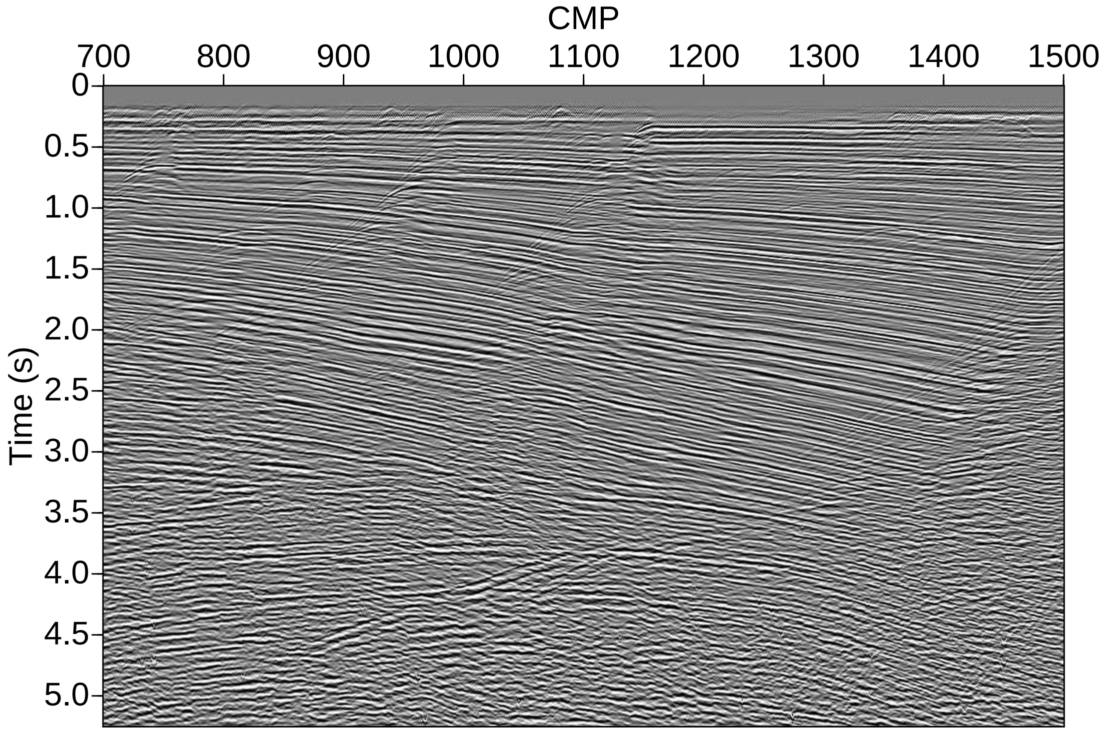

Figure 1: Stacked section from offshore Trinidad, after applying NMO and isotropic homogeneous DMO. The NMO correction is based on the velocities provided by Amoco. tariq2-dmoisi [NR]

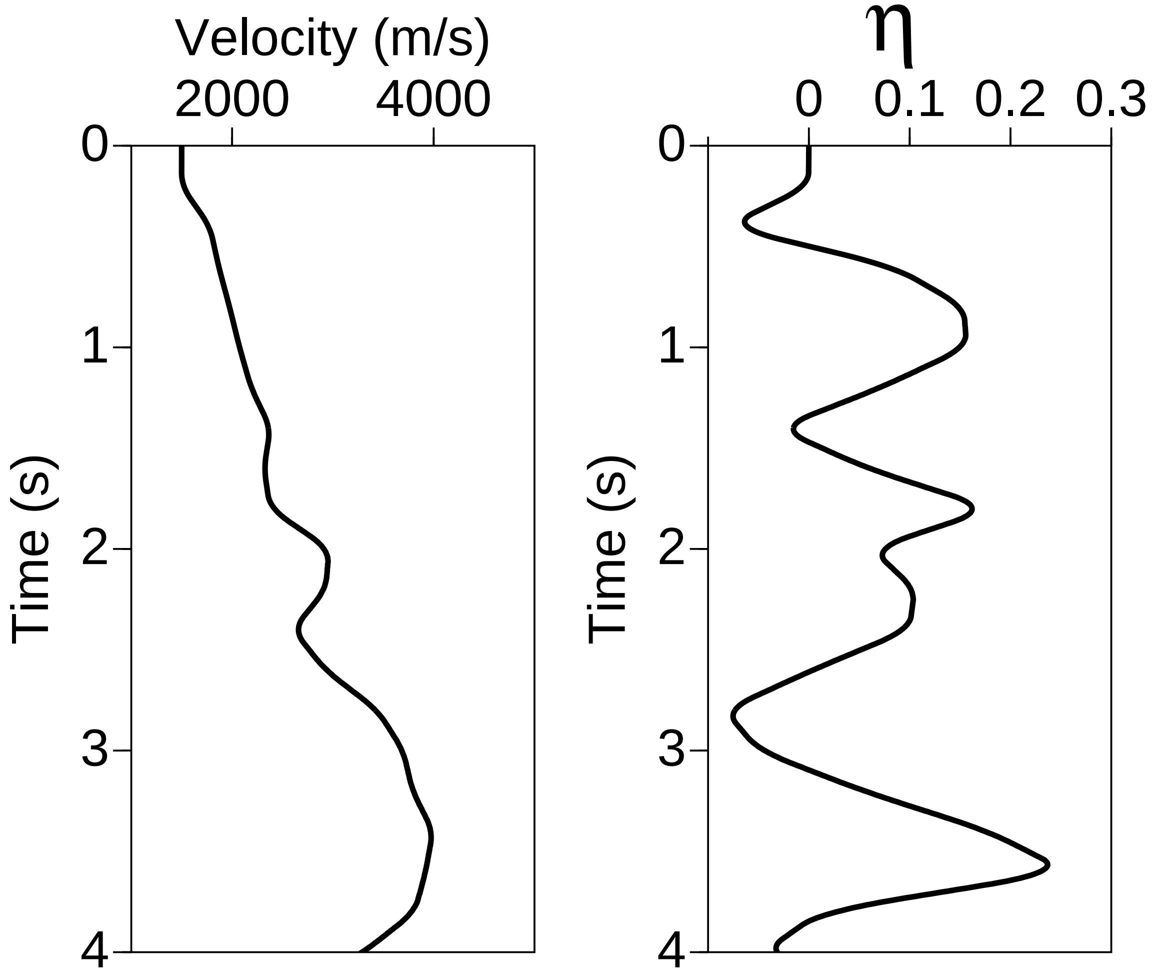

Figure 2: Estimated interval values $v_{\rm nmo}$ and η as a function of vertical time. tariq2-etav1100 [NR]

Carrying out the inversion process described by Alkhalifah (1997a), using the measured values of stacking velocities and corresponding ray parameters, we obtain the functions $v_{\rm nmo}(\tau)$ and $\eta(\tau)$ shown in Figure 2. The inversion assumes no lateral velocity variation in the region of the picks; the lateral velocity variation in this region, especially in the first 2 s, is exceptionally small (see Figure 10). In the water layer, $v_{\rm nmo}$ is 1.5 km/s and η is zero. The accuracy of these estimated curves of $v_{\rm nmo}$ and η depends on the accuracy of the stacking-velocity estimates for both dipping and horizontal reflectors, as discussed by Alkhalifah and Tsvankin (1995).

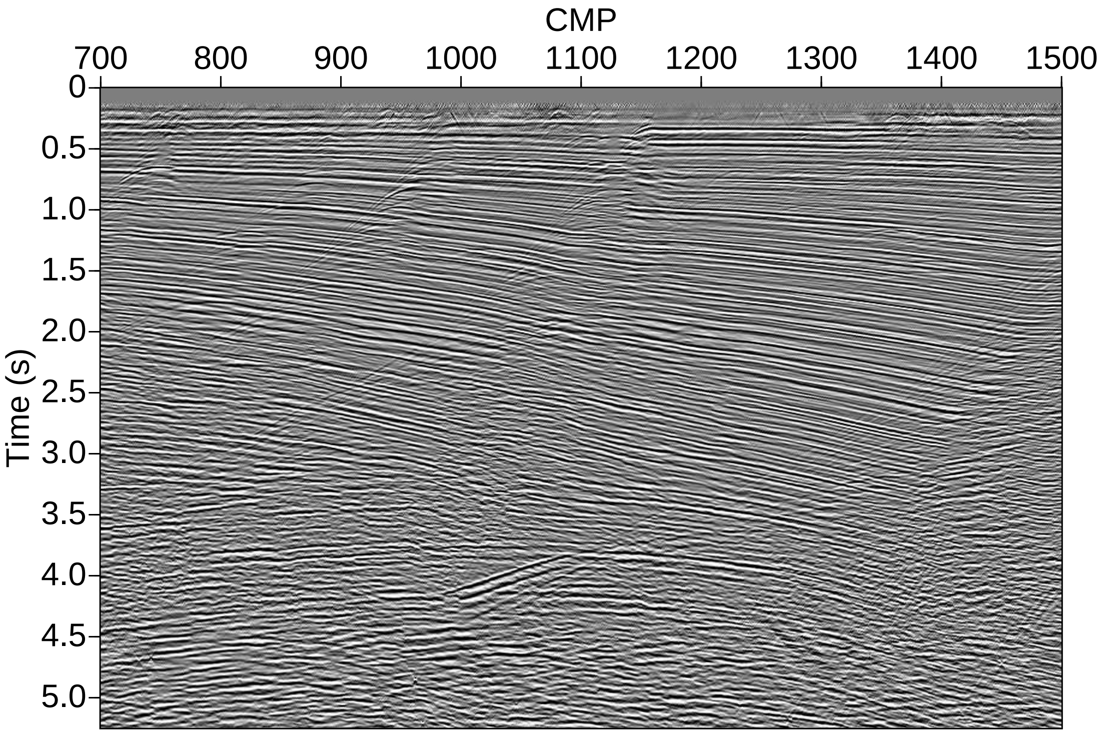

Figure 3: Stacked section after $v(z)$ anisotropic DMO using the parameters in Figure 2. The NMO correction is based on the velocities obtained from the conventional velocity analysis using exceptionally short spreads. tariq2-dmotii [NR]

The smoothed interval values of η in Figure 2 show variations that might depend on the shale-sand long-wavelength alterations. Specifically, shales are expected to induce anisotropic behavior (Banik, 1984; Sayers, 1994) of waves, while sands are usually isotropic. This η curve best fits the measured stacking velocities, and thus is expected to improve the image. The measurement that resulted in Figure 2 corresponds to the fault under CMP location 1100. Later we will examine results from other faults.

Next, we apply a DMO algorithm that uses the derived functions $v_{\rm nmo}(\tau)$ and

$\eta(\tau)$ in Figure 2. Figure 3 shows the result of TI DMO applied to the data, based on the ray-tracing DMO algorithm described by Alkhalifah (1996). Compared with the results of the isotropic DMO given in Figure 1, this section should be improved. A closer look at Figures 1 and 3 (shown in Figures 4 and 5) shows such improvements. In Figure 4 note the vast improvement in focusing both the dipping fault and the sub-horizontal reflections in the anisotropic DMO result (Figure 4b), as opposed to the isotropic one (Figure 4a). Such improvements in focusing are also observed at later times (i.e., Figure 5).

Figure 6 shows CMP gathers from CMP location 936, which contains the imaged fault-plane reflection shown in Figure 4a after (a) homogeneous isotropic DMO, and (b) $v(z)$ VTI DMO. The arrows point to the time of the fault reflection at this CMP location. Whereas the $v(z)$ VTI DMO aligns the fault reflection well, the dipping event after isotropic DMO is misaligned. Improvements are also achieved for sub-horizontal events where DMO managed to correct for the non-hyperbolic moveout that is often largest for small dips.

Although the reflections shown on the seismic line correspond to features within or near the vertical 2-D plane that contains the sources and receivers, some events may represent out-of-plane reflections that require 3-D processing. These out-of-plane reflections, as mentioned earlier, might be expected to stack better at a lower velocity (closer to the isotropic NMO velocity), and therefore focus better in the isotropic image. However, contamination due to out-of-plane events is not expected to be significant for these lines.

Figure 7 show time-migrated sections after (a) isotropic processing, and (b) VTI processing using the inverted parameters shown in Figure 2. Although some improvements in the VTI results can be detected from this figure, a closeup look given by Figure 8 clearly demonstrates the improved imaging achieved by considering anisotropy. Presence of fault plane reflections suggest that the fault is probably a potential reservoir seal. Faults that generate reflections will probably have experienced sufficient movement to cause juxtaposition of different lithologies across the fault plane. These reflections are typically attenuated and/or lost by isotropic processing, while anisotropic processing is successful at preserving these fault plane images.

Three large faults can be picked from the section in Figure 3. Independent estimates for interval η are made at each of these faults. Figure 9 shows the three interval η curves super imposed on the migrated section from Figure 7a. Because the left most fault shows relatively little throw, the corresponding η curve lacks the detail evident in the other two curves, especially at depth. Note, the correlation among the three interval η curves agrees well with the continuity of seismic reflections across the section. The lateral correlation of interval η increases confidence that a geologic parameter is represented by the inversion. Correlation of interval η estimates across faults could help to remove ambiguity in determining correlation of seismic picks across a seismic section.

To demonstrate the mild lateral velocity variation that exists in this region, Fig-

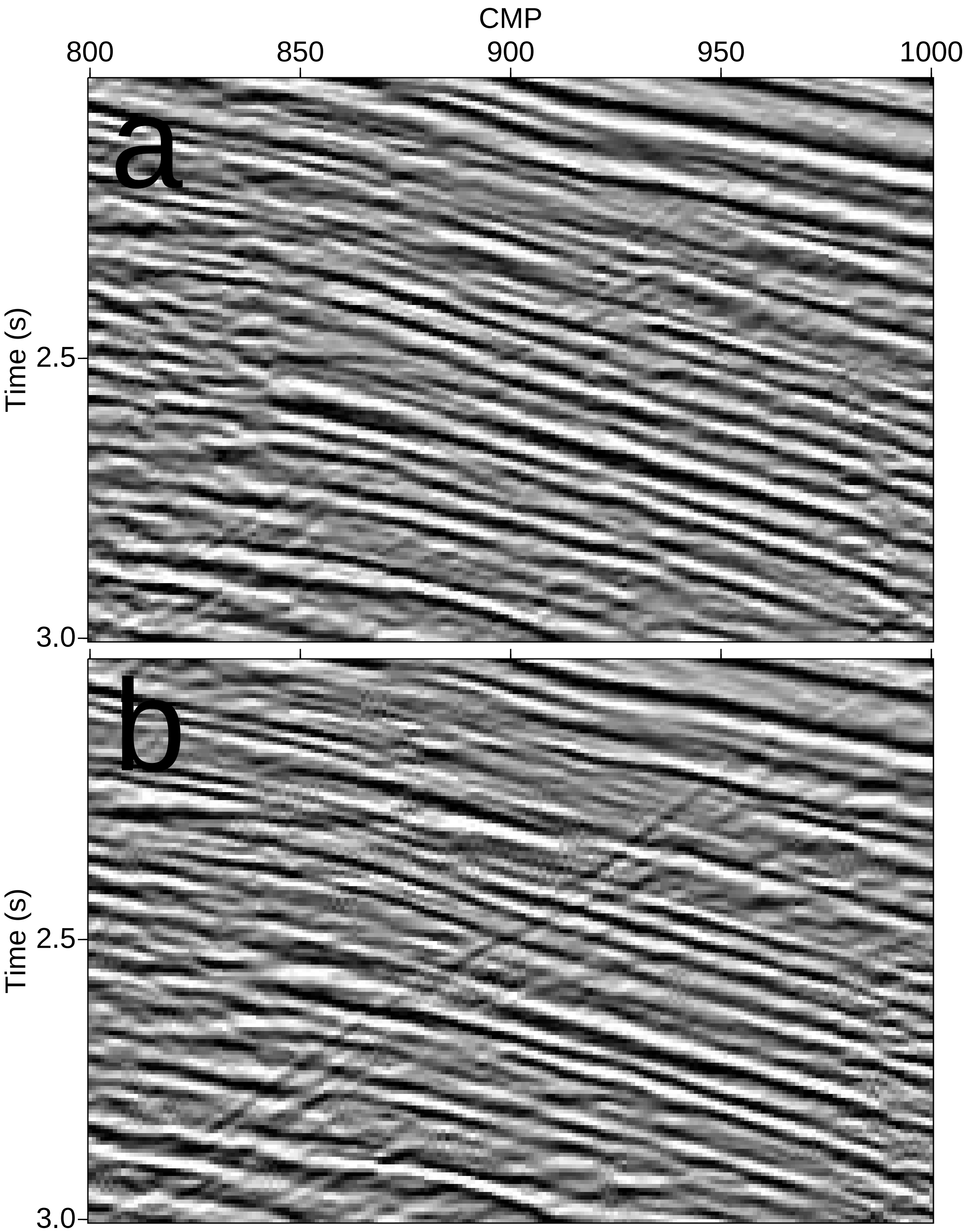

Figure 4: (a) Detail of Figure 1, and (b) detail of Figure 3 in the same region. tariq2-Amococ1 [NR]

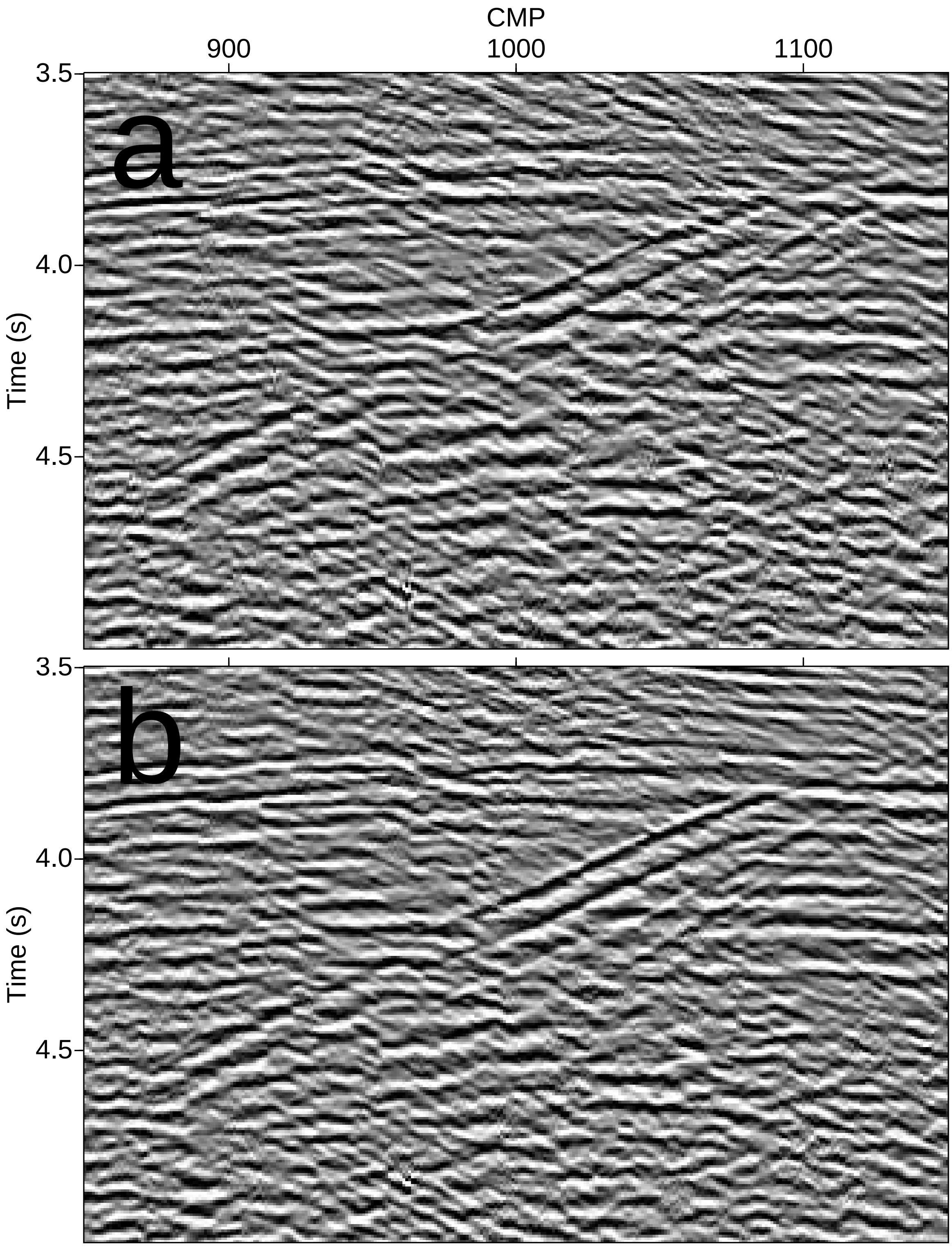

Figure 5: (a) Detail of Figure 1, and (b) detail of Figure 3 in the same region. tariq2-Amococ2 [NR]

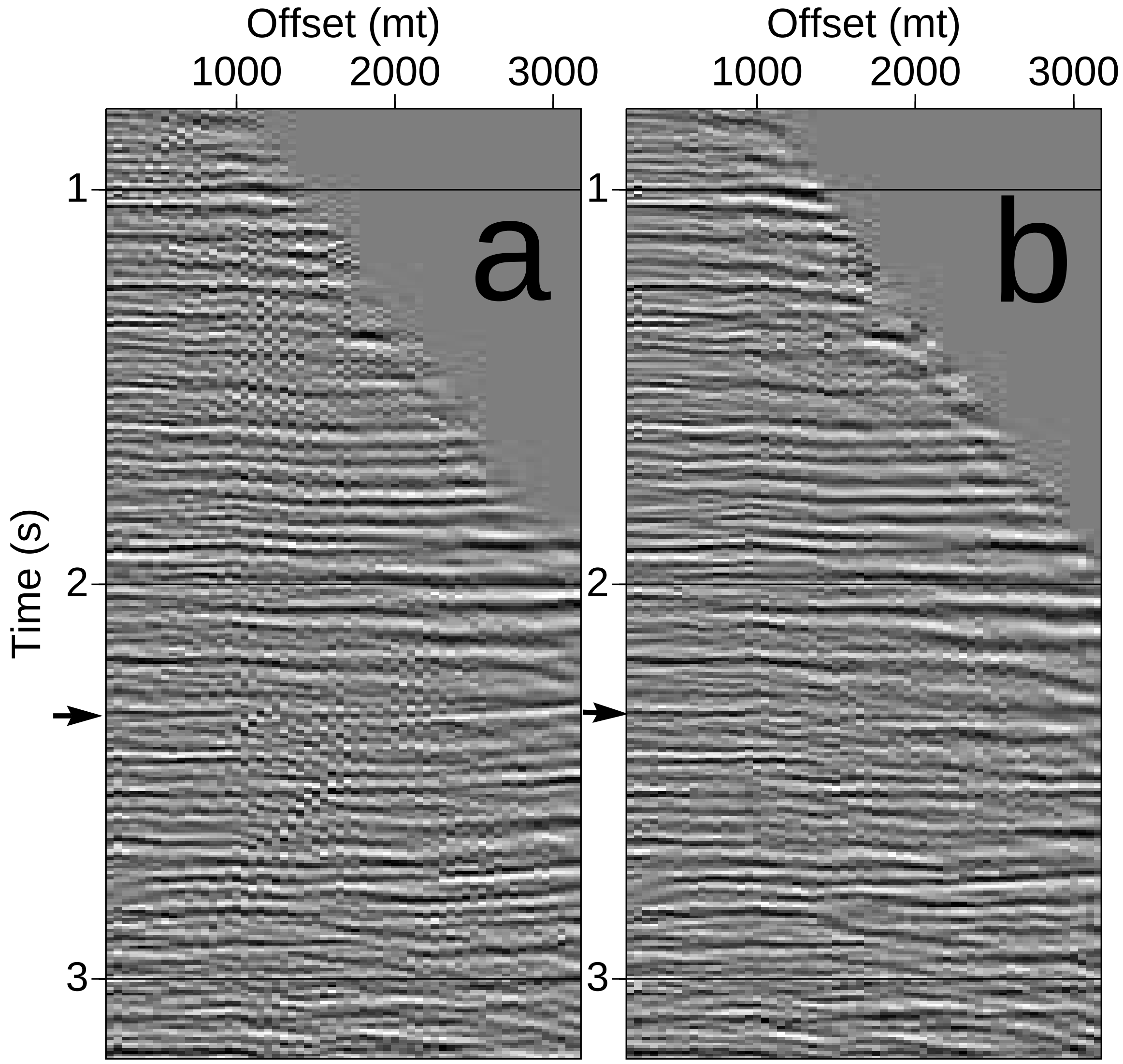

Figure 6: CMP gathers for CMP location 936 after (a) homogeneous isotropic DMO, and (b) $v(z)$ anisotropic DMO using the parameters estimated in Figure 2. The NMO correction for the isotropic DMO result is based on velocities provided by Amoco, while the NMO correction for the anisotropic DMO is based on the velocities obtained from velocity analysis using short spreads. The arrow points to the time of the dipping fault reflection. tariq2-cmpTOZ936 [NR]

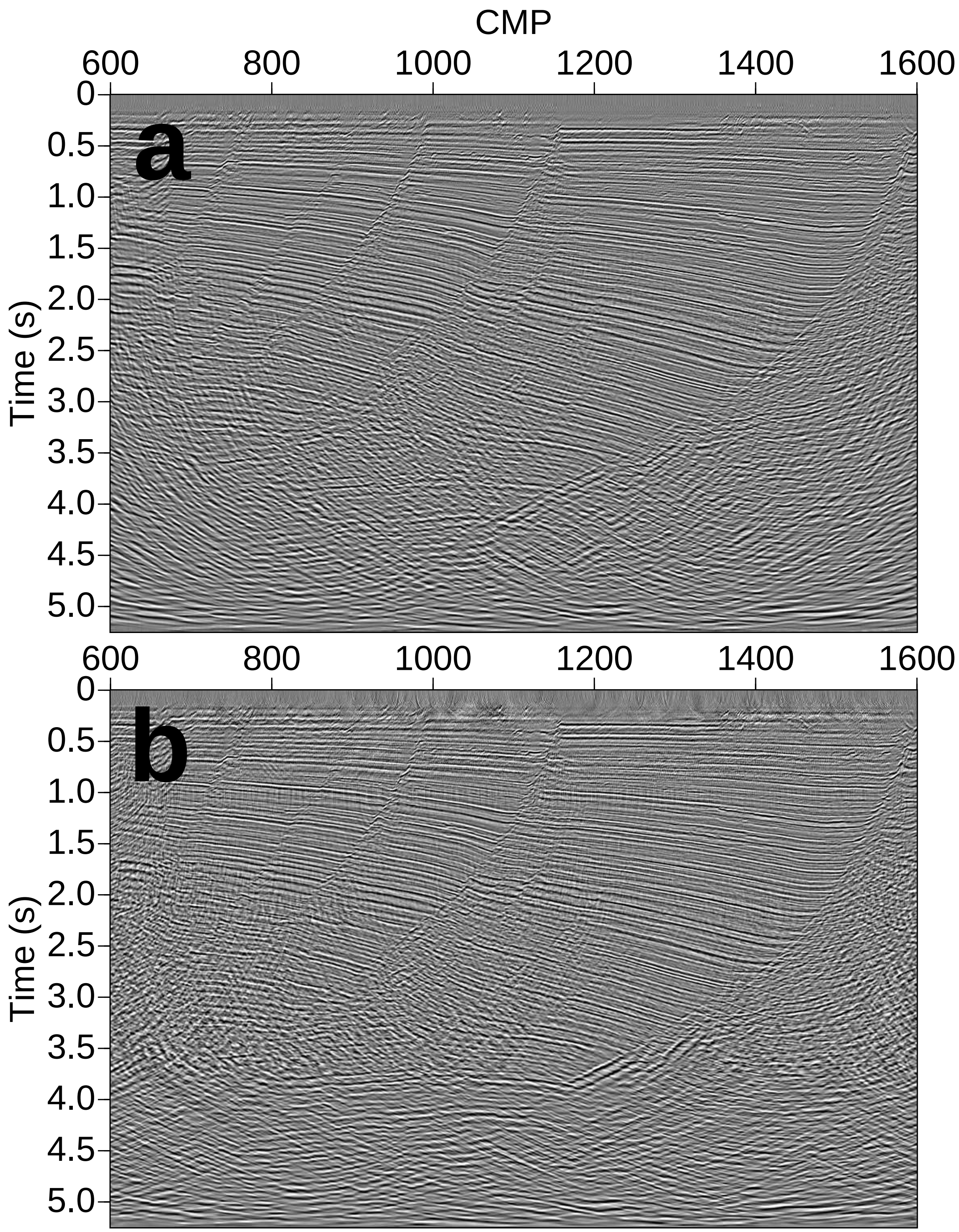

Figure 7: Time-migrated sections after (a) isotropic processing, and (b) VTI processing using the inverted parameters shown in Figure 2. A detailed picture is shown in Figure 8. tariq2-mig1 [NR]

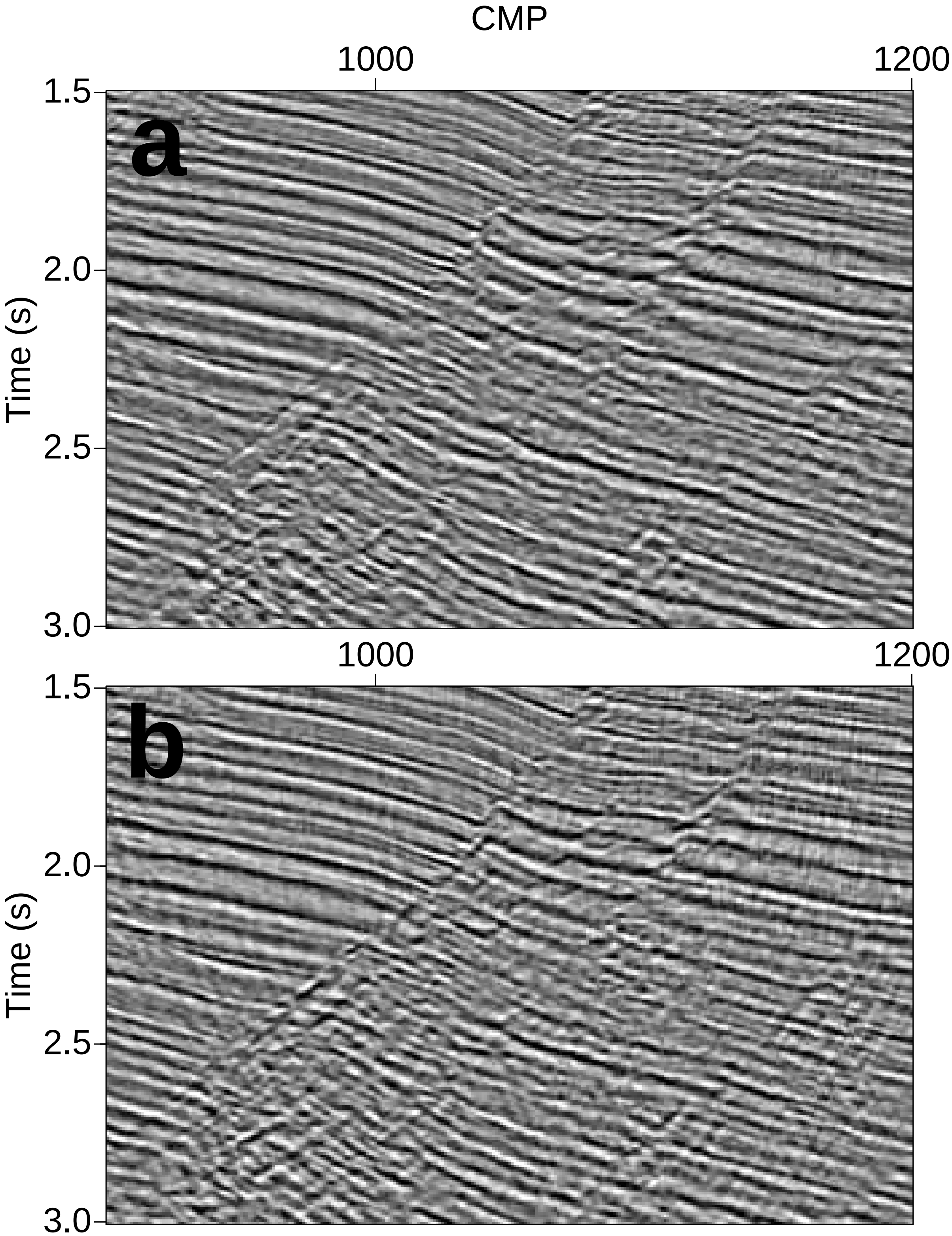

Figure 8: A detailed picture of Figure 7 of time-migrated sections after (a) isotropic processing, and (b) VTI processing. tariq2-migc1 [NR]

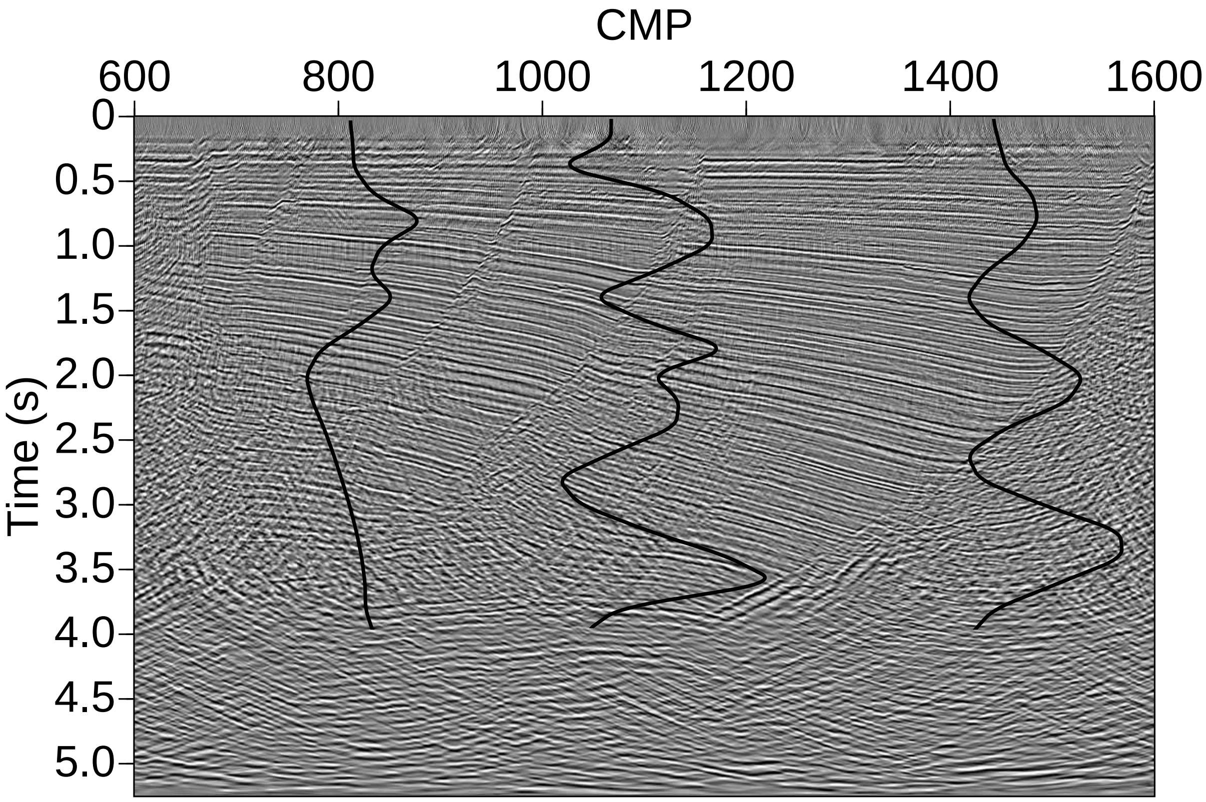

Figure 9: Three interval η curves superimposed on the time-migrated section of Figure 7b. These values correspond to the region above each fault. tariq2-etacurvesmig [NR]

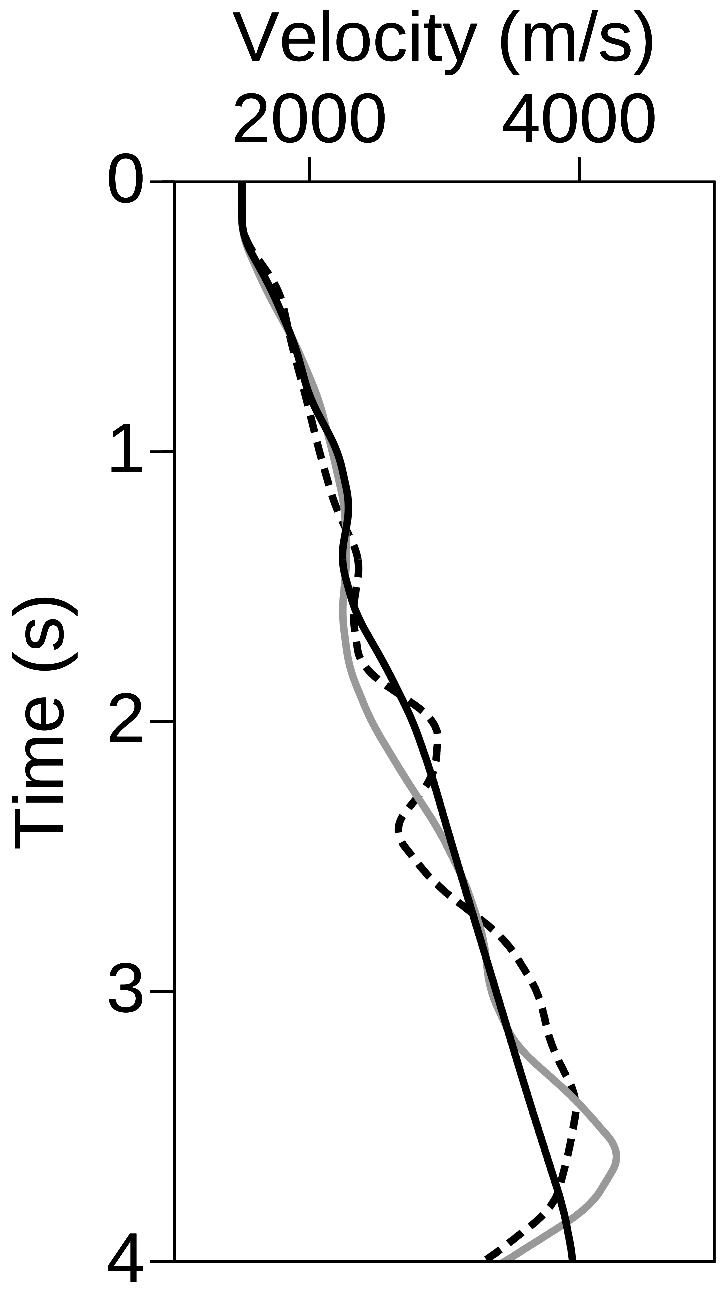

Figure 10: Three interval velocity curves obtained from CMP locations 800 (black solid curve), CMP location 1100 (dashed curve), CMP location 1300 (gray curve). tariq2-vall [NR]

ure 10 shows interval velocities obtained from three separate CMP locations that are more than 2.5 km apart. Velocity changes are insignificant down to 2.0 seconds, and remain very small even at later times.

The second line

Figure 11 shows a zero-offset section that contains a large number of faults. Because of the large offsets present in this data set, we will use the non-hyperbolic method to invert for η. VTI media induce non-hyperbolic moveout of reflections that depends on $V_{\rm nmo}$ and η at large offsets. This non-hyperbolic moveout is used to invert for these two parameters, which provide important information about the subsurface. The direct output from such an inversion (or velocity analysis) is effective values of $V_{\rm nmo}$ and η, that include the combined (average) influence of the overburden. These effective values are converted to interval ones using layer-stripping equations given by Alkhalifah (1997b).

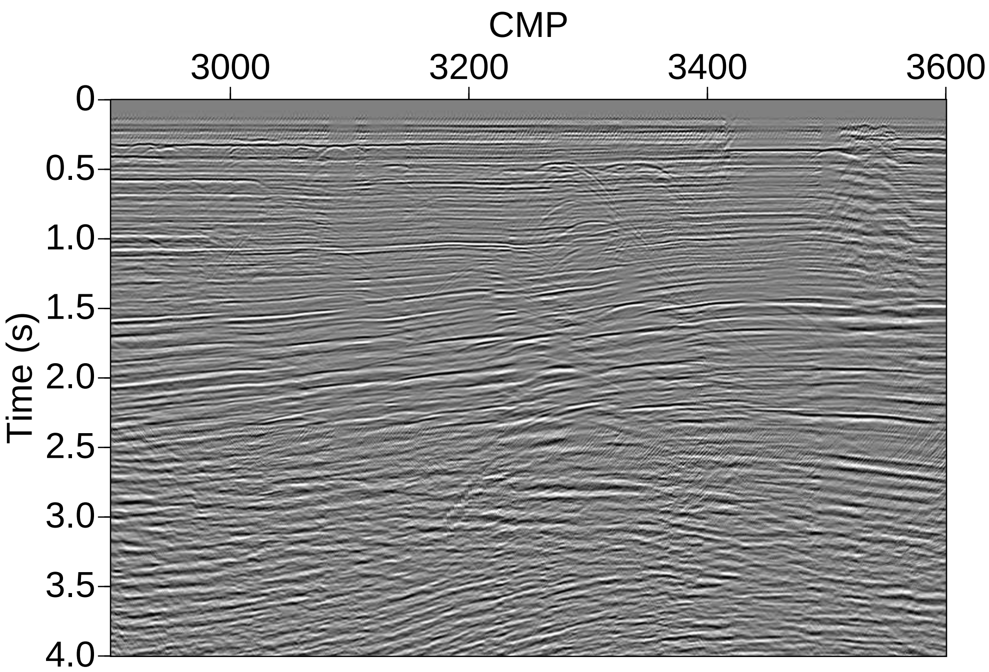

Figure 11: Stacked section of a second line from offshore Trinidad, after applying NMO and isotropic homogeneous DMO. The NMO correction is based on the velocities provided by Amoco. tariq2-dmois [NR]

Figure 12 shows a detail of CMP gather 3100 with a reflection from a horizontal event and the reflection are NMO corrected using different stacking velocities. The highest amplitude stack trace (stack power) is obtained using a velocity of 2100 m/s. Using this velocity, however, did not result in the best resolution of the stacked trace as indicated by the amplitude spectrum. Better resolution (higher-frequency content) is achieved at a lower velocity. However, the best solution is obtained through anisotropic processing as shown in Figure 13, where the non-hyperbolic moveout in the data is treated. A shift in the zero offset time of more than 10 ms from its true value (as given by the near-offset trace) occurs after stacking the 2100 m/s NMO-corrected data. Clearly, a hyperbolic moveout approximation does not adequately approximate the non-hyperbolic moveout represented in the data. This non-hyperbolic moveout can not be explained solely by vertical velocity variations. Furthermore, the lateral inhomogeneity that is apparent in these data by observing velocities from various CMP locations is not sufficient to explain such a large non-hyperbolic moveout.

Figure 14 shows the interval velocity and η values extracted from the non-hyperbolic moveout inversion for CMP location 3200. Considering that the lateral inhomogeneity is small, we will use these values to do VTI DMO and time migration on the whole section (time processing). The extremely high η value at time 1.5 s is indicative of a highly anisotropic shale layer. Also, due to the integral relation between the interval values and the effective ones, the area under these η curves, representing the cumulative anisotropy, tells a better story of the anisotropic impact on the seismic data than the values for the individual intervals. The presence of a thick, highly anisotropic shale at relatively shallow depths (i.e., above zones of interest) will have a serious impact on the effective anisotropy for all deeper layers. If this shallow anisotropy is not taken into account in this case, then degradation of the entire stacked section will result. Figure 15 shows the result of anisotropic DMO and when comparing it with Figure 11 the improvements in focusing the horizontal, as well as the dipping reflections, are obvious.

Figure 16a shows the result of isotropic migration on the isotropically DMO corrected data, while Figure 16b shows the results of a complete VTI processing, including migration. A closer look given by Figure 17 shows the improvement in fault imaging achieved with the VTI processing.

Figure 18 shows three η curves superimposed on the migrated section from Figure 16b. These η curves correspond to CMP locations 3000, 3200, and 3400, and as a result they are placed in their respective positions in the Figure 18. Recognizing that the η highs and lows correspond to reflections from the bottom of the layer that caused these highs or lows, a crude blocky interpretation of the curves can be made and is given in Figure 19. The lateral correlation between these curves that are 2.5 km of lateral distance apart is remarkable. Especially remarkable is the correlation between the thickness of the shale layers and the size of η (look at the first laterally continuous shale layer). The extremely high η value at time 1.5 s is indicative of a highly anisotropic shale layer. While the actual value may appear unreasonable, CMPs 3200 and 3400 are over a gas field, while CMP 3000 is outside of the field (Figure 20). The high η values over the field could suggest vertical migration of the gas into the unconsolidated shale (this shale is approximately 2000 feet thick at depths

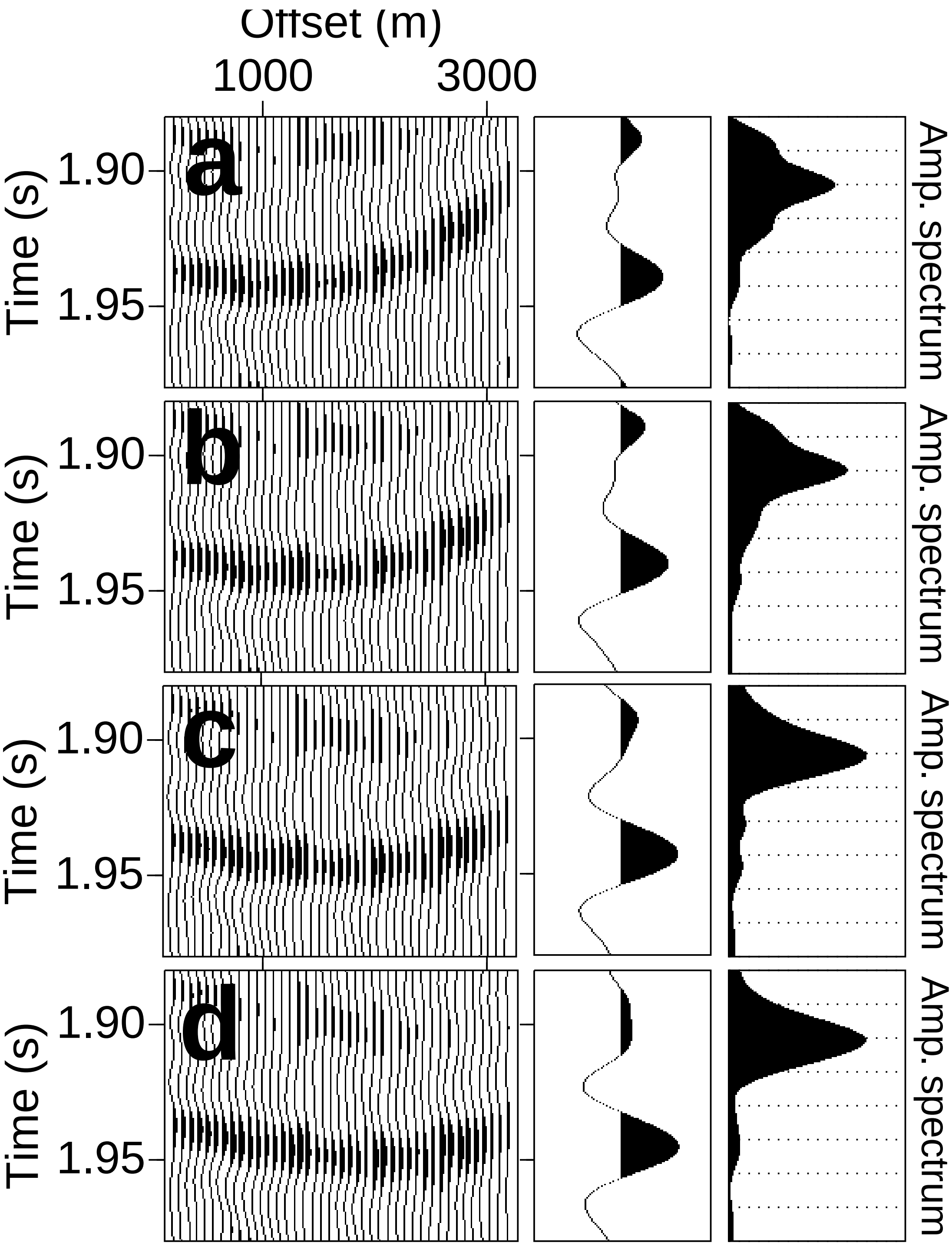

Figure 12: CMP gathers for CMP location 3100 after NMO correction with (a) $V_{\rm nmo}$=2060 m/s, (b) $V_{\rm nmo}$=2080 m/s, (c) $V_{\rm nmo}$=2100 m/s, and (d) $V_{\rm nmo}$=2120 m/s. The first column to the left is the CMP gather, the center column is the stack of the CMP gather, and right most column shows the amplitude spectrum of the stacked gather. tariq2-nmostackf [NR]

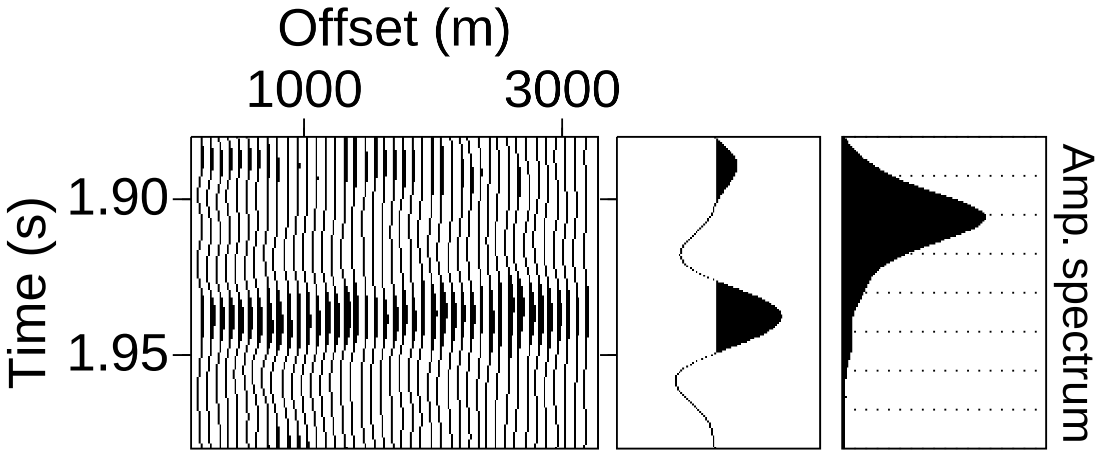

Figure 13: The CMP gather of Figure 12 after non-hyperbolic correction. The first plot to the left is the CMP gather, the center plot is the stack of the CMP gather, and right most plot shows the amplitude spectrum of the stacked gather. tariq2-nmostackfti [NR]

of 3000-5000 feet, see Figure 15).

Figure 20 shows a crude lithologic interpretation estimated solely from the anisotropic inversion. The interpretation is based on the fact that shales are anisotropic, and therefore exhibit large positive η values, while sands are essentially isotropic with near zero values of η. Figure 14 shows the correlation between the estimate for η at CMP 3200 and a blocky interpretation of shale volume from the gamma-ray log at a nearby well. Correlation is remarkably good down to 2.0 seconds, demonstrating the value of using the inversion for η as a lithology estimator. Correlation is not as good below 2.0 seconds, though the v_{nmo} value shown in Figure 21 shows a large decrease in velocity below 2.0 seconds indicative of entering the overpressure zone (which could also impact anisotropy).

DISCUSSION AND CONCLUSION

There are two major advantages of using anisotropic processing over isotropic processing on seismic data. One advantage concerns the quality of the final image: anisotropic processing in areas that contain critical amounts of shale in the subsurface yields better images than isotropic processing. The improvements include better focusing and imaging (positioning) of faults, as well as better focusing of stratigraphic imaging as evidenced by the enhanced continuity of horizontal reflections. The second advantage is an interpretation one: the η curves obtained through anisotropic processing provide us with important lithological estimation tool, used here to distinguish

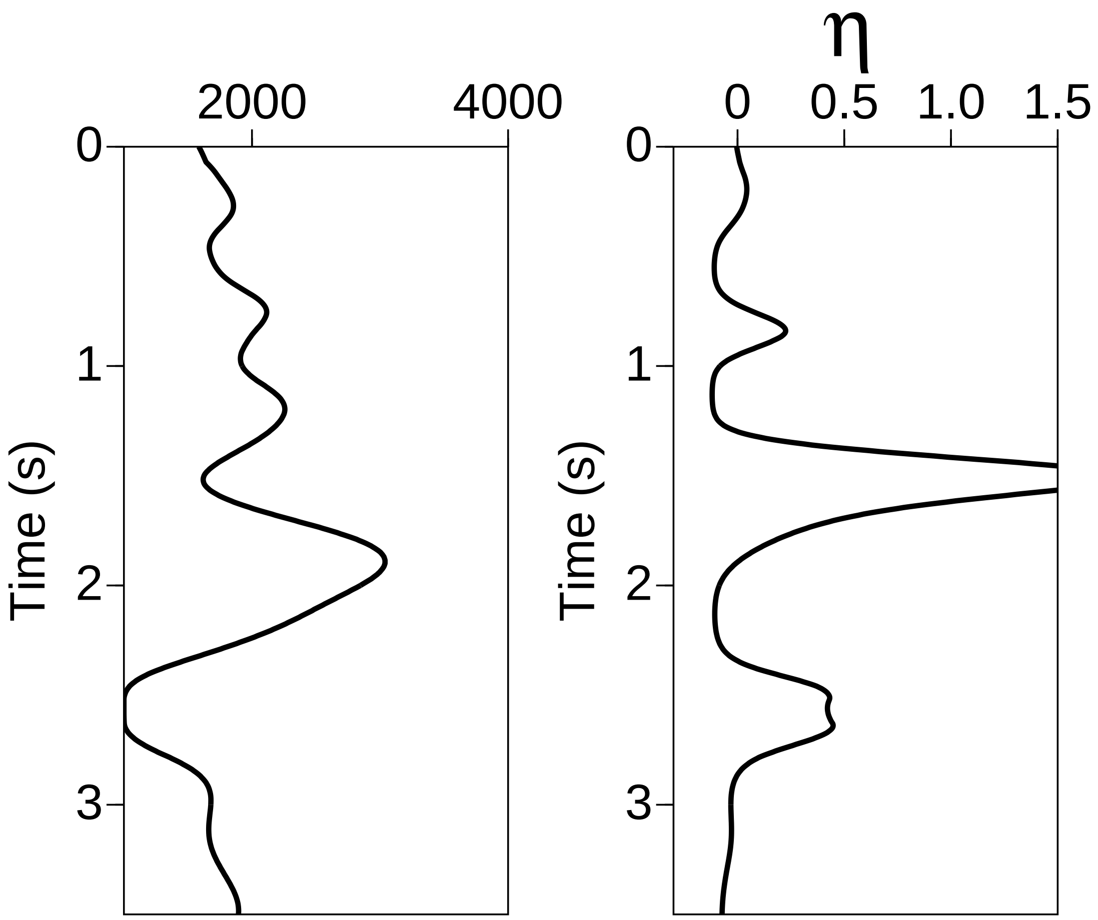

Figure 14: Estimated interval values v_{nmo} and η as a function of vertical time. tariq2-etav [NR]

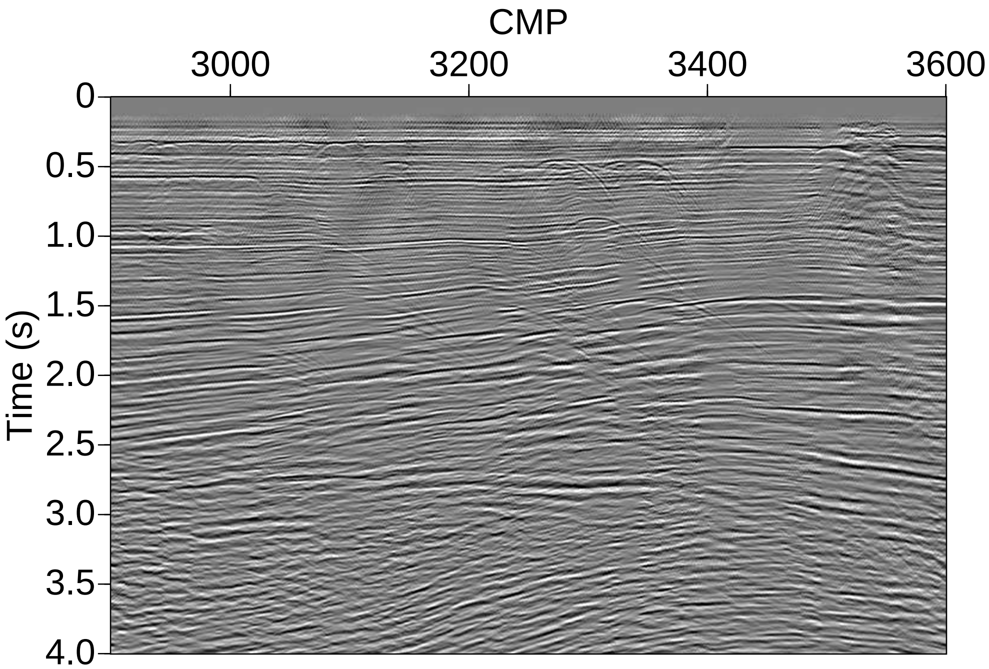

Figure 15: Stacked section after $v(z)$ anisotropic DMO using the parameters in Figure 14. The NMO correction is based on the velocities obtained from the conventional velocity analysis using exceptionally short spreads. tariq2-dmoti [NR]

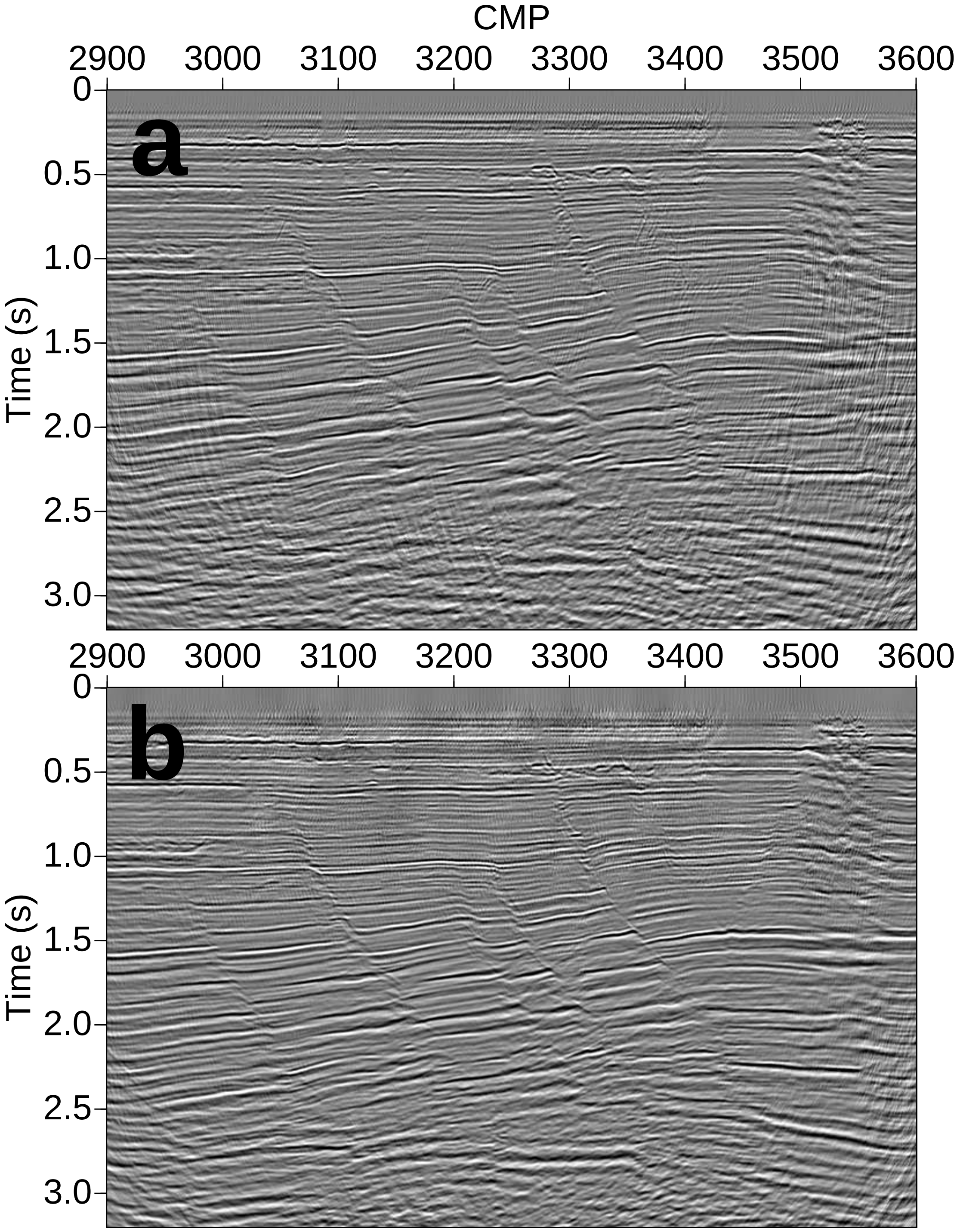

Figure 16: Time-migrated sections after (a) isotropic processing, and (b) VTI processing using the inverted parameters shown in Figure 14. A detailed picture is shown in Figure 17. tariq2-mig [NR]

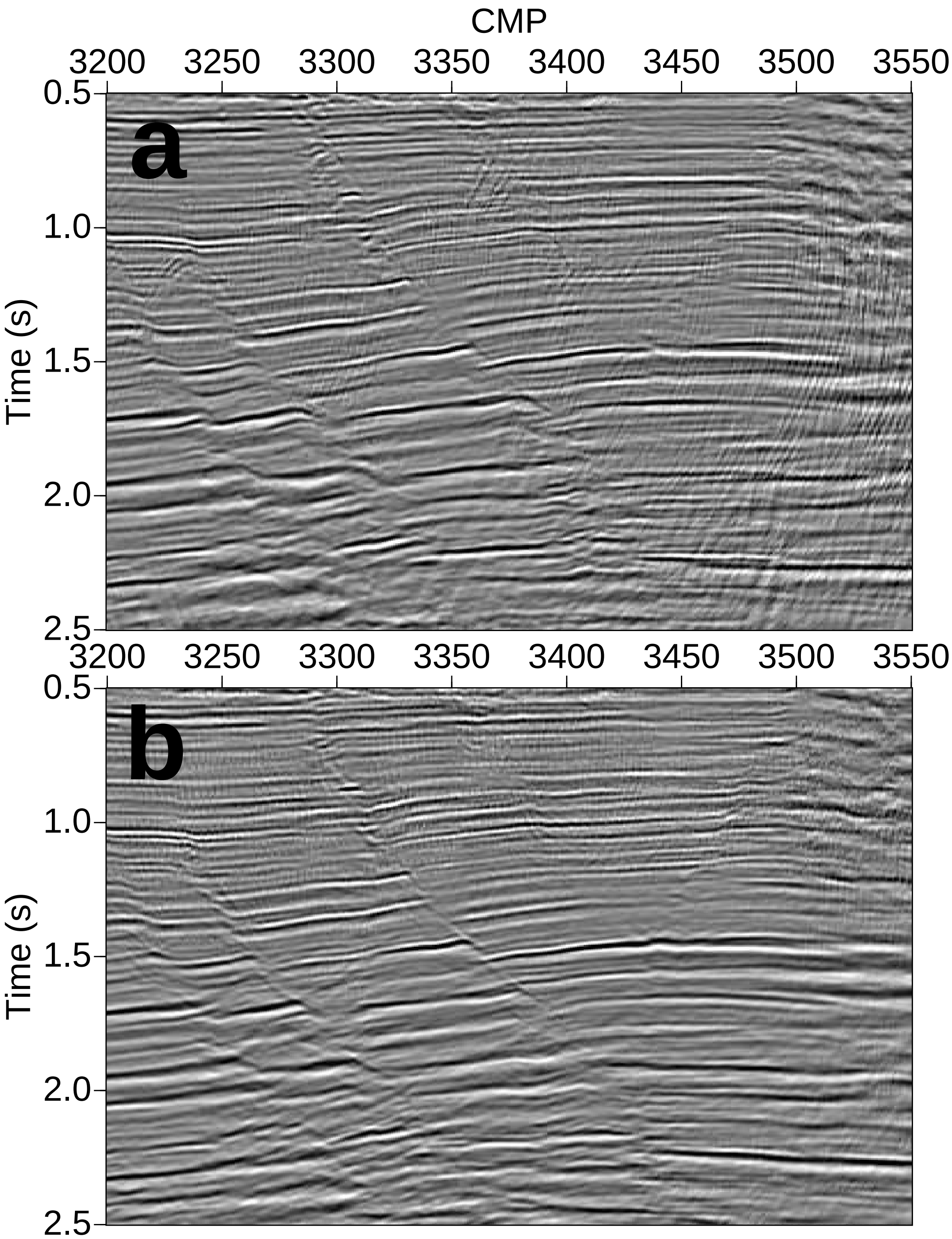

Figure 17: Detail of Figure 16 consisting of time-migrated sections after (a) isotropic processing, and (b) VTI processing. tariq2-migc [NR]

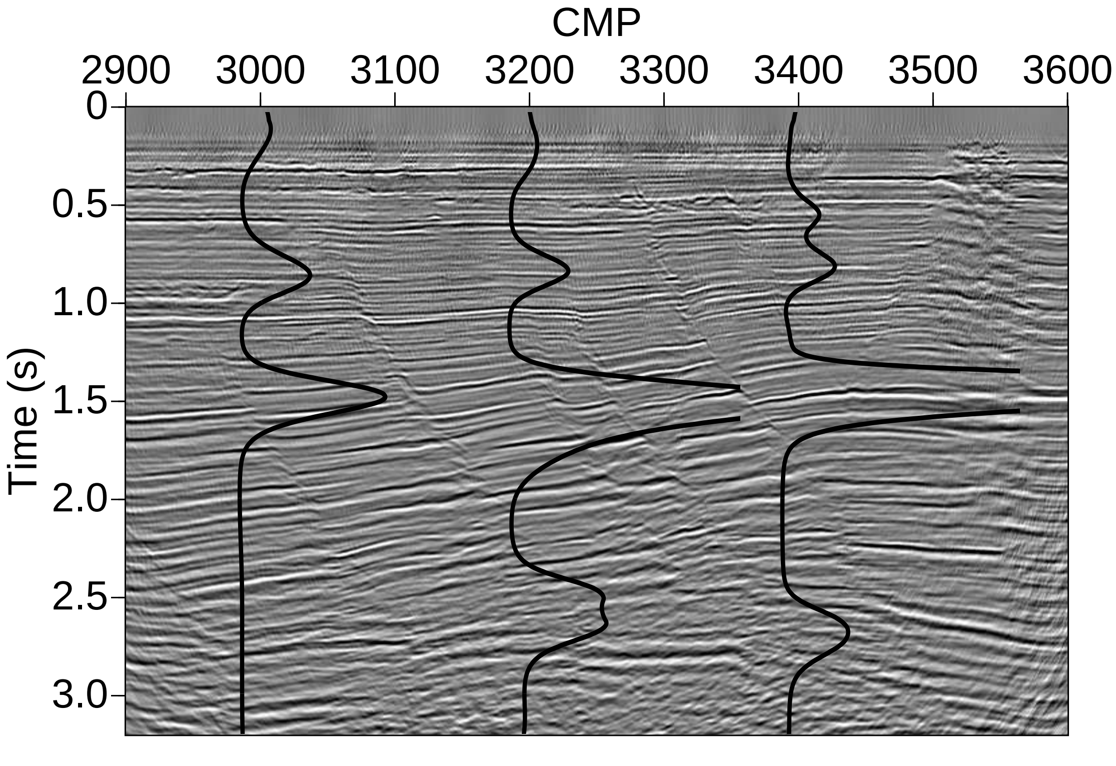

Figure 18: Three interval η curves superimposed on the time-migrated section of Figure 16b. These η values correspond to the region above each fault. tariq2-etacurvesmig2 [NR]

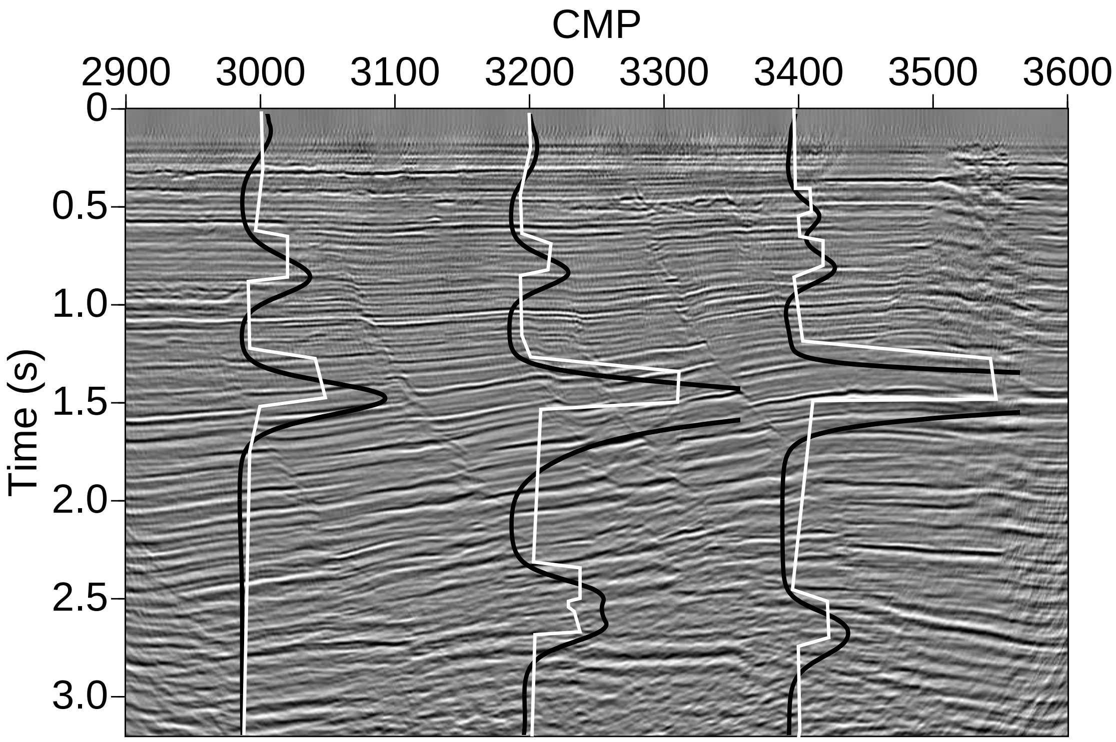

Figure 19: The same three interval η curves shown in Figure 18. The white curves correspond to a crude interpretation of the layering in the subsurface that correspond to the η curves. tariq2-etadismig [NR]

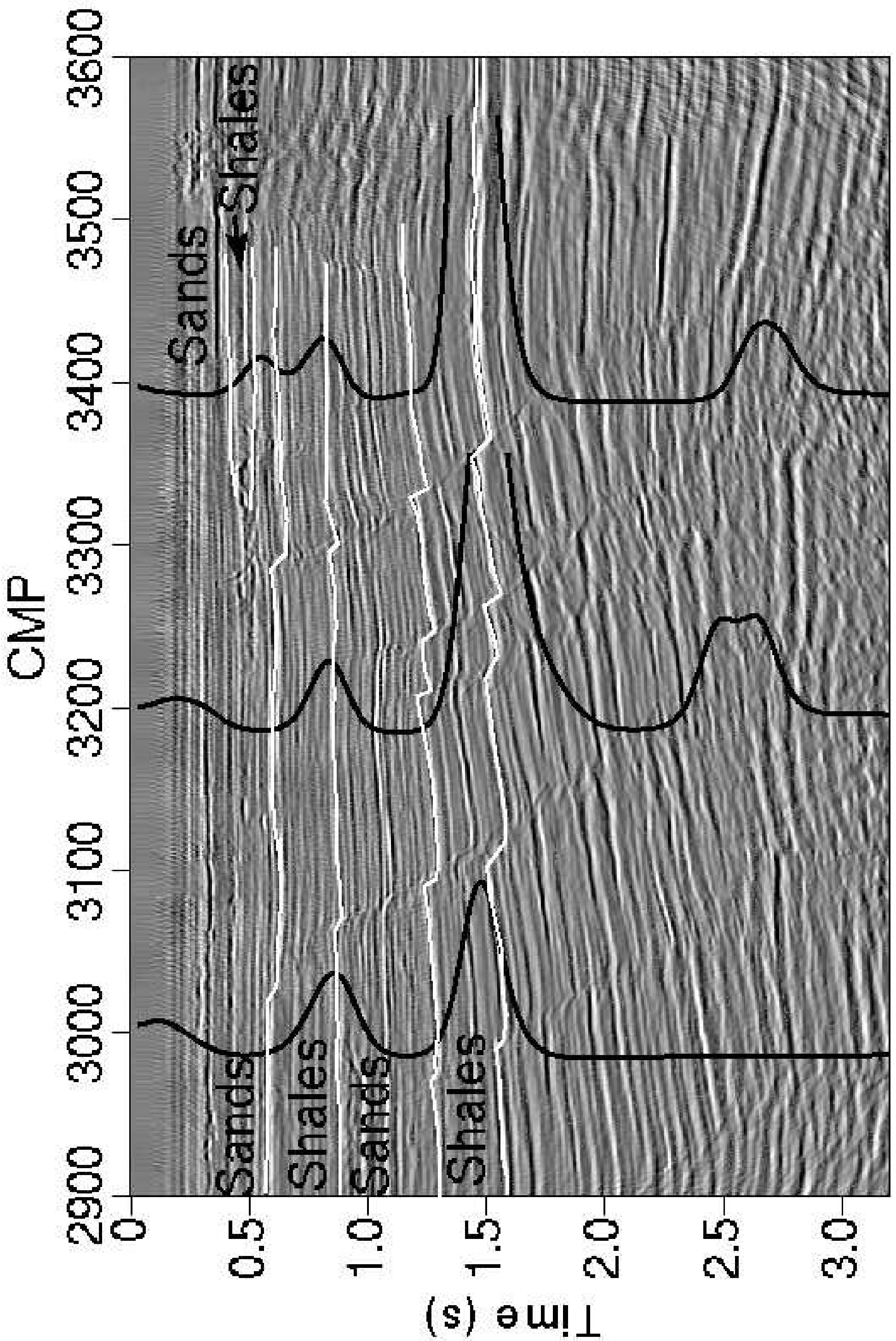

Figure 20: Lithological interpretation of the sand and shale content of the surface as estimated by the interval η values obtained from the inversion. The white lateral lines follow seismic reflections. tariq2-etalayermig2 [NR]

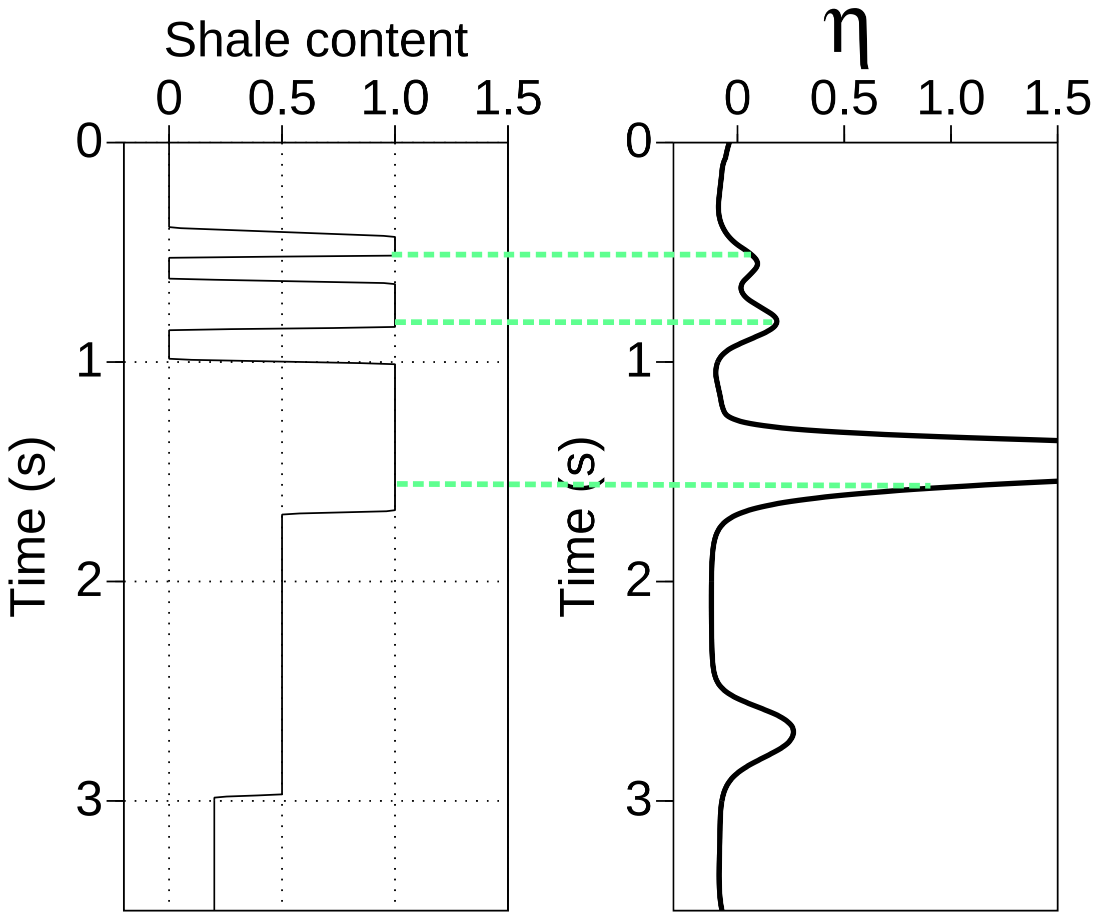

Figure 21: Estimated interval values η plotted next to an approximate long wavelength of shale content extracted from gamma-ray measurements. The gray dashed lines correspond to bottom of shale layer predicted by the η curve and agrees well with the gamma-ray information. $\boxed{\text{tariq2-comparsh}}$ [NR]

between sand-dominated layers and shale-dominated ones.

The imaging benefits of anisotropic processing have been demonstrated previously, but the potential of using the geologic parameter η for lithology estimation shows great potential in current exploration activity. Correlation with gamma ray curves demonstrates the ability to estimate sand and shale dominated intervals in the subsurface. One potential application is in deep water exploration areas where reservoir presence can be difficult to determine. With deep water well costs increasing, additional information that can reduce drilling risk is extremely important. This technique does not require expensive or unusual acquisition procedures—the only requirement is a new look at existing data using refined processing techniques that incorporate real geologic parameters.

REFERENCES

Alkhalifah, T., 1996, Transformation to zero offset in transversely isotropic media: Geophysics, **61**, 947-963.

Alkhalifah, T., 1997a, Seismic Data Processing in vertically inhomogeneo us TI media: Geophysics, **62**, 662-675.

Alkhalifah, T., 1997b, Velocity analysis using non-hyperbolic moveout in transversely isotropic media: Geophysics, in press.

Alkhalifah, T., and Tsvankin, I., 1995, Velocity analysis for transversely isotropic media: Geophysics, **60**, 1550-1566.

Banik, N. C., 1984, Velocity anisotropy of shales and depth estimation in the North Sea basin: Geophysics, **49**, 1411–1419.

Hale, D., 1984, Dip-moveout by Fourier transform: Geophysics, **49**, 741-757.

Lynn, W., Gonzalez, A., and MacKay, S., 1991, Where are the fault-plane reflections?, 61st Ann. Internat. Mtg., Soc. Expl. Geophys., Expanded Abstracts, 1151–1154.

Notfors, C.D., and Godfrey, R.J., 1987, Dip moveout in the frequency-wavenumber domain: Geophysics, **52**, 1718-1721.

Sayers, C.M., 1994, The elastic anisotropy of shales: J. Geophys. Res., **99**, No. B1, 767-774.

Thomsen, L., 1986, Weak elastic anisotropy: Geophysics, **51**, 1954–1966